Paper IV

Double-resonance SAW filters

J. Meltaus, S. S. Hong, O. Holmgren,
K. Kokkonen, and V. P. Plessky

IV

Copyright© IEEE. Reprinted with permission.

This material is posted here with permission of the IEEE. Such permission of the IEEE does not in any way imply IEEE endorsement of any of Helsinki University of Technology's products or services. Internal or personal use of this material is permitted. However, permission to reprint/republish this material for advertising or promotional purposes or for creating new collective works for resale or redistribution must be obtained from the IEEE by writing to pubs-permissions@ieee.org.

By choosing to view this document, you agree to all provisions of the copyright laws protecting it.

Double-Resonance SAW Filters

Johanna Meltaus, *Student Member, IEEE,* Seong Su Hong, Olli Holmgren, *Student Member, IEEE,* Kimmo Kokkonen, and Victor P. Plessky, *Senior Member, IEEE*

***Abstract*— A novel surface acoustic wave filter on a leaky-wave substrate is studied. It features a hiccup-type resonance occurring around a distributed gap between two long interdigital transducers. Compared to a classical coupled resonator filter, it enables a relatively narrow passband (1% to 2% of center frequency) with low insertion loss, steep skirts and improved suppression levels. The structure consists of long transducers having the number of fingers greater than $1/K^2$ and $1/\kappa$, where K^2 is the coupling coefficient of the substrate material and κ is the reflectivity per wavelength, separated with short transducer sections constituting a distributed gap. A strong, localized resonance is formed in the gap region, in addition to the resonance arising in the long structures - hence the name "double-resonance filter". The substrate studied here is 42°-rotated lithium tantalite. We show experimental results for both single-ended and unbalanced-to-balanced filters at 1.6 GHz, having a minimum insertion loss of 1.07 dB, suppressions of 30 dB and absolute -3-dB bandwidth of 29 MHz (1.9% of the center frequency). For the balanced device, the amplitude imbalance over the passband ranges from -0.6 dB to 2 dB and the phase imbalance from 1° to 4.5°. Furthermore, we have measured the acoustical power distributions using a scanning laser interferometer, and compare these results with the profiles simulated using a coupling-of-modes model.**

I. Introduction

LONGITUDINALLY coupled surface acoustic wave (SAW) filters (CRF, also referred to as dual-mode SAW filters, or DMS) [1] feature a wide passband (3%–5% of center frequency) with low insertion loss (IL), relatively high suppression levels outside the passband and a straightforward way of obtaining balanced-unbalanced (BALUN) operation. Such devices typically have several acoustically-coupled, relatively short interdigital transducers (IDT), giving rise to interfering resonance modes that constitute the filter response. They are currently widely used in, e.g., mobile telecommunications applications.

A simple CRF having 2 or 3 transducers often has insufficient suppression close to the high-frequency edge of the passband. Although this effect can be countered by increasing the number of transducers or by using a series resonator to improve the suppression [2], CRFs typically have filter roll-off that is not as steep as what can be obtained with some competing topologies, such as ladder filters. Another drawback associated with the CRF structure is the resistive loss arising from the relatively wide aperture, typically 50λ–100λ, especially at high frequencies (above 1 GHz). The aperture can be decreased if several tracks are connected in parallel [3] or if the number of fingers is increased [4].

The passband width of CRFs is basically determined by the coupling coefficient, K^2, of the piezoelectric substrate. It is difficult not only to increase the passband but also to decrease it, simultaneously retaining low IL and good shape of the transfer curve. Therefore, the design of low-loss filters having 1% to 2% passband can be difficult, as suitable substrate materials are not readily available.

We study a novel filter structure consisting of long IDTs separated by a "distributed gap" realized in a form of short transducers with reduced pitch. Experimental results of filters at 1.6 GHz featuring 1% to 2% passband width on a leaky-wave 42°-$LiTaO_3$ substrate are presented. This structure yields a low insertion loss typically on the order of 1.5 dB in the passband, a steep filter roll-off, and suppression levels below -30 dB. The operation of the structure is based on a localized resonance that is developed in and around the distributed gaps. There also exists a synchronous resonance arising in the long transducers; therefore, we call the structure a double-resonance filter (DRF). We discuss the operation of the device and present experimental results for both single-ended and balun filters.

II. Operation of the Double Resonance Devices

A. Double-Resonance Structure

A coupled SAW filter featuring unconventionally long transducers was first proposed by Plessky *et al.* in 1996 [5]. Although simulations promised excellent narrow-band filter performance on leaky-wave substrates, realized devices suffered from high IL and poor transfer curve shape. A similar device with improved loss levels was later realized by S. S. Hong [6]. The topology studied in the present work is similar to that presented in [5] except for that gaps are replaced with distributed gaps, i.e., the phase change conventionally occurring in a metallized gap is realized with short transducer sections. The pitch of the short IDTs is selected so that the necessary phase shift is obtained; typically it should be smaller than in the main IDTs so as to avoid generation of bulk-acoustic waves (BAW) [4], [7]. It has been shown [7] that for leaky-wave substrates, especially for 42°-$LiTaO_3$ optimal for SAW propagation under a grating, the distributed gap considerably reduces propagation and bulk-wave conversion loss. It has been demonstrated experimentally that high Q-values around $Q = 600$ can be achieved [8].

The topology studied in the present paper is schematically illustrated in Fig. 1. The filter consists of relatively short

Manuscript received February 24, 2006.

J. Meltaus is with Helsinki University of Technology, Espoo, Finland (phone: +358-9-451 5740, fax: +358-9-451 3164, e-mail: Johanna.Meltaus@tkk.fi).

S. S. Hong is with Samsung Electro-Mechanics Co, Ltd., Suwon, Korea.

O. Holmgren and K. Kokkonen are with Helsinki University of Technology, Espoo, Finland.

V. P. Plessky is with GVR Trade SA, Bevaix, Switzerland, and with Helsinki University of Technology, Espoo, Finland (e-mail: Victor.Plessky@bluewin.ch).

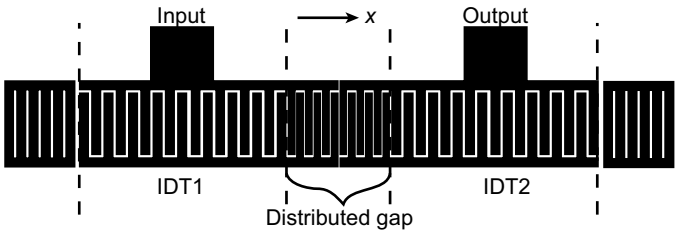

Fig. 1. Topology of a symmetric 2-IDT double resonance filter. Between the long transducers (IDT1 and IDT2) there is a distributed gap consisting of short transducer sections. Between reflector and IDT, no gap is used.

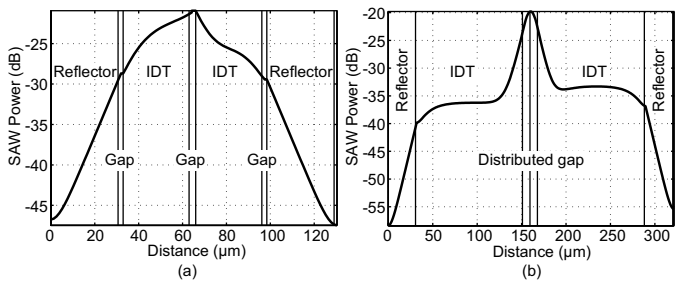

Fig. 2. Calculated distributions of acoustic wave power at the center frequency of a conventional 2-IDT CRF with 25 fingers in both IDTs (a) and a 2-IDT DRF (b). In the conventional CRF, the SAW energy is distributed in the IDTs, whereas in the DRF design, the main part of the energy is concentrated around the gap region.

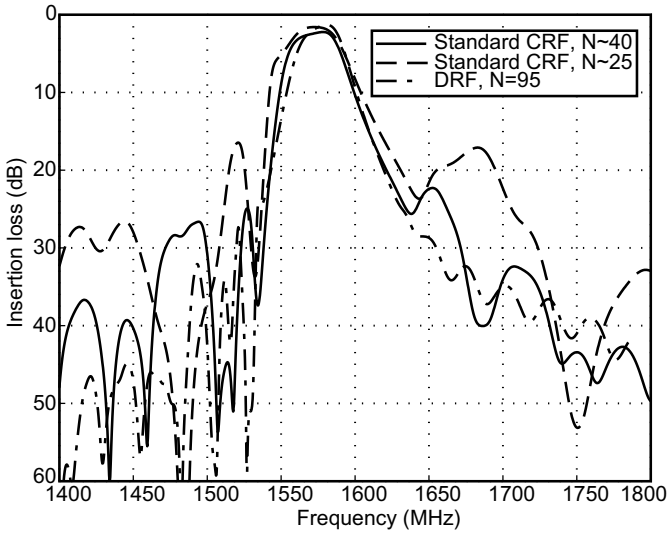

Fig. 3. Calculated frequency responses for standard 2-IDT CRF (solid and dashed line) and a 2-IDT DRF (dash-dotted line). The DRF structure features a narrower passband and higher suppression levels than the conventional CRF.

reflectors surrounding two long transducer structures separated by a distributed gap. There are no gaps between the reflectors and the IDTs. Although the filter studied here is symmetric, it is not necessary. The number of fingers, N, in the IDTs is substantially greater than $1/K^2$ and $1/\kappa$, where K^2 is the coupling coefficient of the substrate and κ is the reflectivity per wavelength; for leaky-wave substrates such as 42°-$LiTaO_3$, $N \gg 50$.

To illustrate the operation principle of a DRF compared to a conventional CRF such as described in [1], Fig. 2 shows coupling-of-modes (COM) model simulations of SAW amplitude distribution at the center frequency in a 2-IDT CRF having N=25 electrodes in both IDTs (a), and in a 2-IDT DRF (b). The corresponding frequency responses are depicted in Fig. 3. The 2-IDT CRF is not optimized for performance; rather, the structure is chosen to produce a response typical of such a device.

In the standard CRF structure of Fig. 2(a), the SAW power is distributed over the whole structure, whereas in the DRF structure in Fig. 2(b), energy is concentrated around the distributed gap region. In a conventional CRF, the acoustic resonance modes arising over the length of the device interact to create the response, whereas in a DRF structure, the resonance forms primarily in the gap. Therefore, care must be taken to counteract the loss mechanisms in the gap region, as they have a significant effect on the operation of the device. In a metallized or free-surface gap, the conversion of SAW into BAW at the edges of periodic structures and propagation loss occurring on the surface of the gap (especially important on 42°-$LiTaO_3$ [9]) attenuate the resonance, deteriorating the performance of the filter and leading to such difficulties as reported in [5].

Simulated curves in Fig. 3 illustrate the differences in the frequency responses of 2-IDT conventional CRF and a DRF. A CRF structure with the number of fingers N=25 in each IDT, shown with the dashed line in Fig. 3, features a relatively wide passband and a characteristic decrease in suppression above the passband, resulting from internal reflections in the IDTs. In a CRF with 40 fingers in each IDT, the lobe above the passband is reduced and the transition band steepness is improved. In a DRF structure with N=95, the transducer band is radically decreased such that the sidelobe disappears and the filter passband is narrower than in conventional CRFs, with sharp transition to rejection band. Long transducers also allow to reduce the aperture compared to a standard CRF, reducing losses arising from the finger resistivity.

B. Resonances in the DRF Structure

Two practically independent resonances occur in a DRF structure such as shown in Fig. 1: a ”synchronous” resonance created in the long IDTs, and a ”hiccup”-type resonance arising in the gap region. Although the structure is quasi-periodic with no visible perturbation in periodicity, we use the term ”hiccup resonator”, introduced by P. Wright for the synchronous structures with an off-set close to $\lambda/4$ between two parts of the IDT [10], [11].

Fig. 4 shows the experimental admittance curves (real and imaginary parts of admittance) of a one-port double-resonance resonator, with a structure similar to that of Fig. 1 having both IDTs connected in parallel. The synchronous resonance arises at 1544 MHz and the hiccup resonance at 1589 MHz. The end of the grating stopband occurs at 1647 MHz, so that the hiccup resonance takes place near the center of the stopband.

In a two-port device such as shown in Fig. 1, the high reflectivity of the long transducers hinders the propagation of the SAW inside the structure from input port to output port. Therefore, the synchronous resonance arising in the input IDT

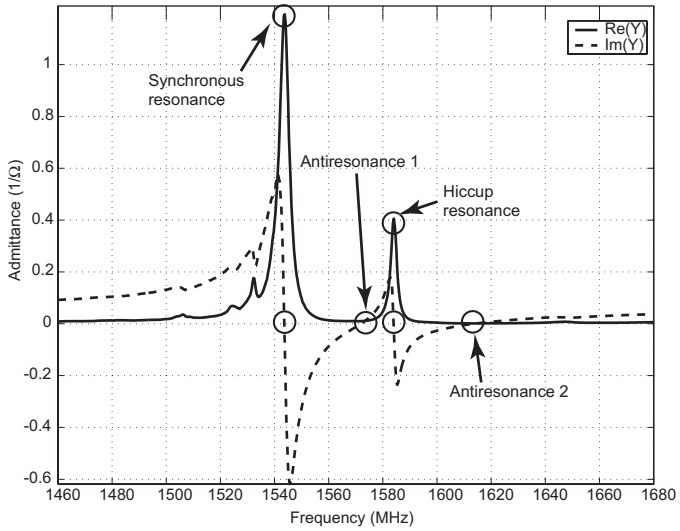

Fig. 4. Experimental admittance curves showing the resonances arising in a one-port DRF structure. Synchronous resonance appears at 1544 MHz and hiccup resonance at 1589 MHz.

is not effectively transferred to the output IDT, and only a weak electrical response is created at this frequency. Only at the hiccup resonance frequency, the strong resonance arising in the gap region serves to transfer energy from the input IDT to the output IDT. Thus, a narrow-band bandpass response with high suppression levels in the filter stopband can be achieved. Experimental data of acoustic power distribution in a DRF structure confirm this hypothesis and will be presented in Section III-B.

As the finite-element method (FEM) simulation of a one-port resonator in Fig. 5(a) shows, the long IDTs determine the strength of the synchronous resonance, leaving the hiccup resonance virtually unaffected. Changing the periods, pt, in the distributed gap alters the position of the hiccup resonance, as measurements of experimental one-port devices show in Fig. 5(b).

C. Self-Matching of the Hiccup Resonance

An interesting feature of the DRF structure is the possibility to intrinsically match the hiccup-type resonance. This effect can be seen in Fig. 5. As the number of fingers N in the main transducers is increased, as in Fig. 5(a), or the hiccup resonance position is shifted, see Fig. 5(b), the anti-resonance point of the synchronous resonance will at some point coincide with the hiccup resonance frequency. In such a situation, the synchronous resonance acts as a matching inductance, canceling the static capacitance of the hiccup resonance and making the response more symmetric. Experimental electrical response of a 2-IDT filter in Fig. 5(c) shows the effect of self-matching on filter passband: as the matching improves, the passband becomes more symmetric and IL reduces. If the periods of the distributed-gap IDTs are further reduced from the self-matched situation, the hiccup resonance becomes again unmatched, and the passband shape deteriorates.

To obtain self-matching, one needs to adjust the length of the long IDTs and the dimensions of the distributed gap region so that the resonance and anti-resonance frequencies coincide. In addition to this, the coupling coefficient, K^2, determining the anti-resonance frequency of the long IDTs and the reflection coefficient, κ, determining the width of the stopband, must be appropriately related for self-matching to be possible. The half-width of the reflector stopband, Δf_{HW}, is determined (relative to the reflector center frequency f_0) by

$$\frac{\Delta f_{HW}}{f_0} = \frac{|\kappa|}{2\pi}. \tag{1}$$

If the hiccup resonance takes place in the middle of the grating stopband, Δf_{HW} must be equal to the resonance-anti-resonance (R-a-R) distance of the synchronous resonance for self-matching to occur. The R-a-R distance (relative to the resonance frequency f_{r}) may be approximated to be

$$\frac{f_{\mathrm{ar}} - f_{\mathrm{r}}}{f_{\mathrm{r}}} \approx \frac{K^2}{2}, \tag{2}$$

where f_{ar} is the anti-resonance frequency. Therefore, the condition for self-matching is approximately

$$K^2 \approx \kappa/\pi. \tag{3}$$

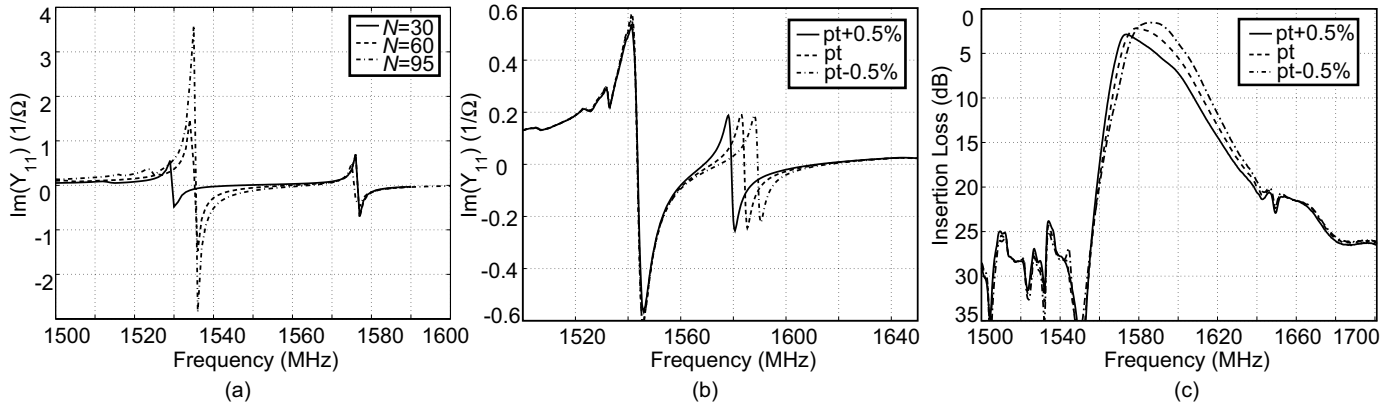

Fig. 5. (a) FEM simulation illustrating the effect of long IDTs (N=number of fingers in IDT) on the strength of the synchronous resonance occurring at 1535 MHz in a one-port resonator. The hiccup resonance at 1575 MHz remains unchanged. (b) Experimental result showing the effect of the period, pt, in the distributed gap on the hiccup resonance frequency. (c) Experimental frequency responses of a 2-IDT DRF as the period in the distributed gap is varied.

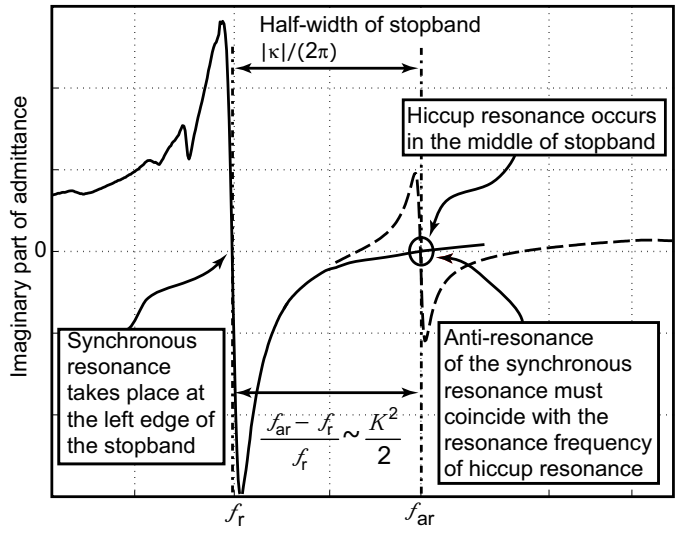

Fig. 6. Principle of self-matching of the hiccup resonance in DRF structures. The anti-resonance of the synchronous resonance acts as a matching inductance for the hiccup resonance, canceling the static capacitance. For self-matching to take place, the half-width of the stopband must equal the resonance-anti-resonance distance of the synchronous resonance, so that its anti-resonance coincides with the hiccup resonance frequency.

TABLE I

DEVICE PARAMETERS AND EXPERIMENTAL CHARACTERISTICS OF THE DOUBLE-RESONANCE FILTERS.

Parameter	2-IDT Filter	3-IDT Filter
Aperture per track (μm)	110 = 43λ	42 = 16λ
Number of fingers in side IDTs	95	95
Number of fingers in gap IDTs	7	7
Number of fingers in middle IDT	-	145
Minimum insertion loss (dB)	1.27	1.07
Absolute 3-dB bandwidth (MHz)	23 (1.48%)	29 (1.9%)
Relative 3-dB bandwidth (MHz)	29 (1.8%)	36 (2.3%)
Suppressions (dB)	30	40
Phase balance (°, absolute 3-dB band)	-	1...4.5
Amplitude balance (dB, absolute 3-dB band)	-	-0.6...2.1

TABLE II

SCAN PARAMETERS FOR THE DETAILED AND ROUGH SCANS.

Parameter	Detailed	Rough
Scan points (y×x)	130 × 1000	88 × 206
Scan step (μm, y×x)	0.99 × 0.33	1.705 × 1.705
Scan area (μm×μm)	129 × 330	150 × 351

To further clarify the self-matching phenomenon, the imaginary part of admittance of a one-port DR resonator, showing the synchronous and hiccup resonances with respect to the reflector stopband, is schematically illustrated in Fig. 6. A relatively strong piezoelectric substrate is required for the self-matching to be obtained. For example for quartz, with $K^2 \approx 0.001$ and $\kappa \approx 0.04$, there is an order of magnitude difference and the self-matching condition cannot be satisfied. On the other hand, for 42°-$LiTaO_3$ with $K^2 \approx 0.05$ and κ ranging from 0.1 to 0.25, depending on the geometry of the finger structure, the condition can be met. If the hiccup resonance is shifted away from the center of stopband, the self-matching condition is modified.

Self-matching of the hiccup resonance is a significant asset in many device applications, improving the device performance and eliminating the need for a matching inductance. The presence of two anti-resonances (the imaginary part of admittance crossing zero, Fig. 6) near the resonance frequency is also of a great convenience in filter design: the anti-resonances can be used to create notch points resulting in steep skirts.

III. EXPERIMENTAL RESULTS

We have fabricated and measured both one-port resonators and narrow-band filters satisfying the specifications used in the Global Positioning System (GPS). The substrate used in this work is 42°-$LiTaO_3$ with metallization thickness of 8% of the wavelength and metallization ratio of 0.6.

A. Samples and Measurements

We have fabricated the following samples: (1) One-port resonator, (2) DRF with 2 IDTs (see Fig. 1), (3) DRF with 3 IDTs and balanced output. The structure of the one-port resonator is similar to that depicted in Fig. 1 with the two ports connected in parallel. The 3-IDT DRF consists of two similar filter tracks connected in parallel, with input in the middle IDT and output in the side IDTs, and the polarity of the output transducers in the second track inverted with respect to the first track to provide balanced output signal.

All samples were electrically probed on-wafer. Device parameters and electrical figures of merit are presented in Table I. In addition to the electrical measurements, for the one-port resonators and 2-IDT filters, we have performed laser-interferometric measurements of the acoustic vibration amplitude distribution.

B. Experimental Amplitude Distributions

In this section, we show experimental SAW amplitude distributions and compare them with the corresponding COM simulations. Experimental data are acquired with a scanning homodyne laser interferometer described in detail in [12]. The interferometer detects mechanical vibrations perpendicular to the surface (vertical component). The relative amplitudes of the surface vibrations obtained with the interferometer correspond to the acoustic power, i.e., when the relative amplitude increases 6 dB, the acoustic displacement is doubled.

In addition to the relative vibration amplitude, the mean intensity of the laser beam reflected from the sample surface is recorded at each scan point. The obtained light intensity values are used to create a microscope-like image of the scanned area (hereafter called light-reflection image). Therefore, there is a one-to-one correspondence between the light-reflection image and the amplitude-data image. It should be noted that amplitudes in areas with different optical reflectivity (e.g., grating and metal surfaces) cannot be directly compared since the sensitivity of the interferometer depends on the reflectivity

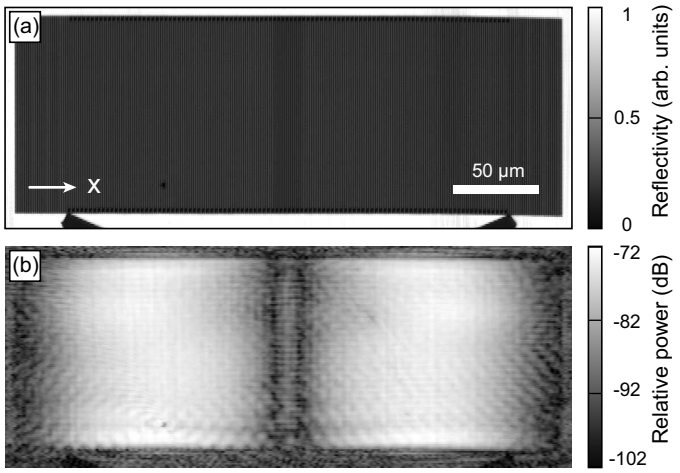

Fig. 7. Laser-interferometric scan at the synchronous resonance frequency (1543 MHz). (a) Light-reflection image of the scanned area, and (b) relative amplitude of the vertical vibration component (Fourier filtered).

of the sample surface.

Laser-interferometric measurements of the one-port resonator were carried out over the frequency range of interest (1480 MHz to 1696 MHz) with a frequency step of 2 MHz in order to disclose the acoustical behaviour of the device. Based on these measurements, 30 most interesting frequencies were selected for more detailed scans. The scan parameters are shown in Table II.

The interferometer data are filtered in Fourier domain to remove the standing wave pattern and the contributions caused by the high and low optical reflectivity of the finger structure. Thereby, the envelope of the acoustic wave fields is obtained. In other words, the measured amplitude distribution, converted to linear scale, is Fourier transformed, and high spatial frequencies corresponding to the periodicity of the finger structure are suppressed. Finally, an inverse Fourier transformation is applied and the filtered data is converted to dB-scale.

A detailed areal scan of the active resonator area at 1543 MHz is shown in Fig. 7. In the light-reflection image (Fig. 7(a)), the finger structure of the transmitting IDTs and the reflector gratings are barely visible. In the amplitude image (Fig. 7(b)), a smooth amplitude profile can be observed after Fourier filtering.

In Fig. 8, 5 line profiles of the measured acoustical power distribution along the propagation direction of the wave (x-direction) are plotted with the corresponding line profiles calculated using the COM model. The experimental line profiles are extracted from the areal scans by averaging 70 longitudinal lines, i.e. lines in the x direction. It should be noted that averaging of longitudinal lines is performed to the data transformed to the linear amplitude scale (not power) before the Fourier filtering.

To facilitate the comparison, the calculated curves are shifted so that the maximum intensity coincides with the maximum intensity of the experimental curves. The experimental relative power levels are comparable at different frequencies,

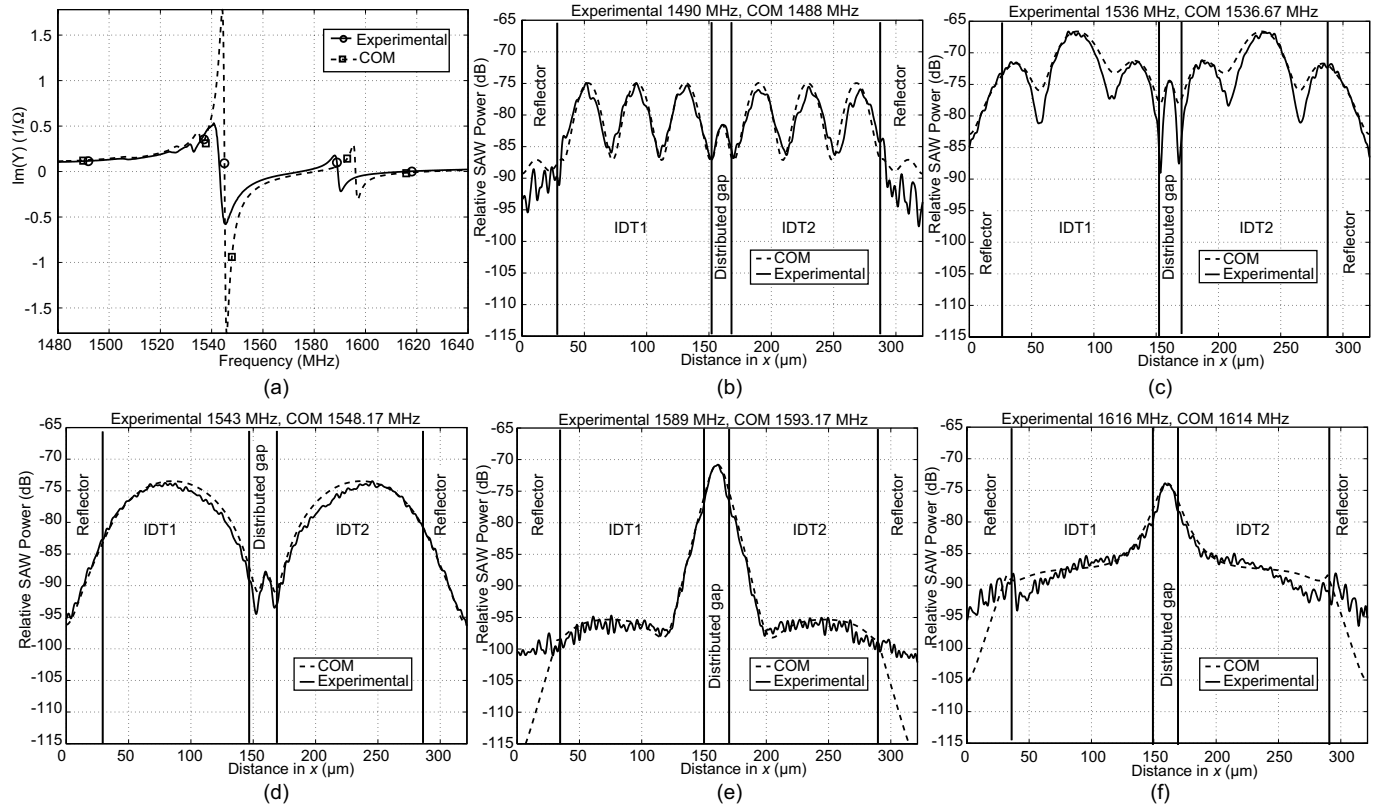

Fig. 8. (a) Electrical response and (b)–(f) Fourier filtered line profiles of the amplitude distribution in the x-direction in the one-port double-resonance resonator. Amplitude distributions shown in (b)–(f) are measured and calculated at the frequencies indicated by circles and squares in (a), respectively.

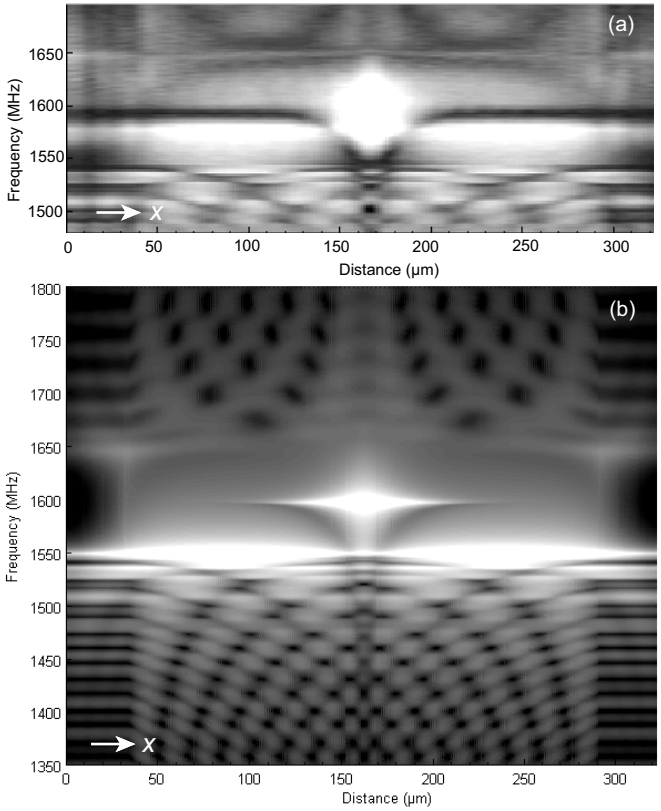

Fig. 9. Mode charts for double-resonance one-port resonator, showing the SAW amplitude distribution on the length of the resonator at each frequency: (a) experimental measurements with the rough scan step, and (b) calculated distributions. The x-axis, oriented in the same way as in Fig. 1 and presented by the arrows in the figures, shows the position on the device. The plot consists of line profiles of SAW amplitude as a function of frequency.

but it should be noted that in Figs. 8(b)–(d), the nominal input power was 20 dBm, whereas in Figs. 8(e)–(f) it was 10 dBm, so as to avoid high acoustic power levels in the gap region.

The imaginary part of measured (solid line) and calculated (dashed line) admittance of the resonator are plotted in Fig. 8(a). On top of the admittance curves are shown the frequencies at which the SAW distributions are investigated: measured (circles) and calculated (squares). The simulated frequencies are slightly different from the experimental ones because they are selected around the measurement frequency so that the best match between the experimental and simulated amplitude distribution is found. The shift between the experimental and simulated frequencies shown in Fig. 8(a) is linear. The slight discrepancy between the simulated and measured electrical response is probably due to parasitic effects, such as stray capacitances and inductances arising from the contact pad layout and the measurement setup, that were not taken into account in the simulations.

Below the grating stopband, mode patterns with multiple nodes arise. The profiles in Figs. 8(b) and (c) show such patterns; with Fig. 8(c) between two modes. The synchronous resonance, with acoustic amplitude distributed in the long transducers, is shown in Fig. 8(d), and the hiccup resonance in Fig. 8(e). The amplitude distribution at the antiresonance frequency is depicted in Fig. 8(f).

In Fig. 9, both experimental (a) and simulated (b) mode charts, summarizing the resonance characteristics of the one-port resonator in the frequency domain, are shown. The x-axis shows the position on the device along the propagation path. At each frequency point, the line profile along the resonator at that frequency, such as in Fig. 8, is plotted using a grayscale color map. The synchronous resonance can be seen around 1550 MHz and hiccup resonance at 1600 MHz. The experimental data depicted in Fig. 9(a) extend from 1480 MHz to 1700 MHz, whereas the simulated frequency range of Fig. 9(b) is wider.

Amplitude distributions in a 2-IDT filter for three distinct frequencies are shown in Fig. 10. In Fig. 10(a), a distribution below the grating stopband is shown. In the input transducer, a mode similar to those seen in the one-port resonator arises, but the acoustic wave does not propagate into the output transducer. Fig. 10(b) depicts the wave field at the synchronous resonance frequency, where the acoustic power is concentrated in the input IDT, and the power transferred to the output IDT is considerably smaller. At the hiccup resonance frequency (Fig. 10(c)), the power levels at the input and output are comparable, and there is a strong concentration of amplitude in the distributed gap area. At and around this frequency,

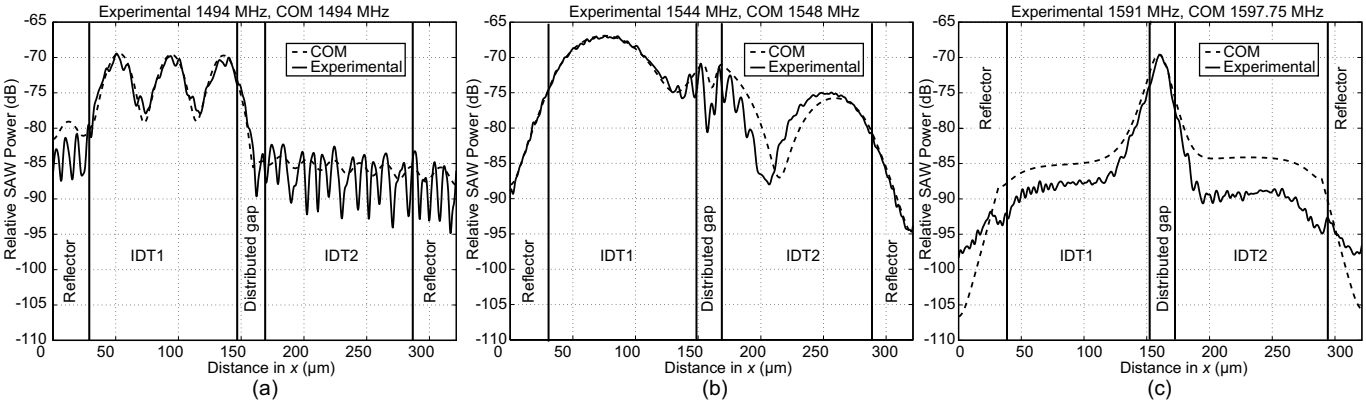

Fig. 10. Simulated (dashed line) and measured (solid line) SAW amplitude distributions in a 2-IDT filter: (a) below the grating stopband, (b) at the synchronous resonance below the filter passband, and (c) at the hiccup resonance, in the filter passband. The simulated curves are shifted so that the maximum power coincides with that of the measurement. The nominal input power level is 20 dBm in (a) and (b) and 10 dBm in (c).

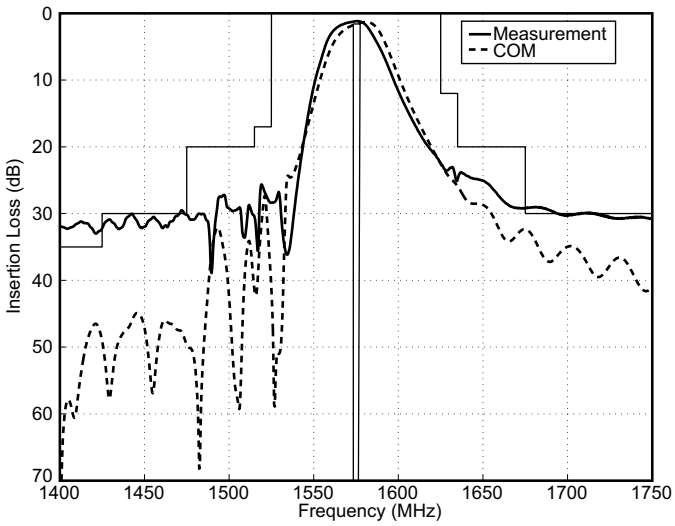

Fig. 11. COM simulation (dashed curve) and measurement (solid curve) of a single-ended 2-IDT double-resonance filter (see Fig. 1). Specifications shown in the figure are for a low-loss GPS filter. Difference in the suppression level between simulation and experiment is due to feedthrough arising from the contact pad topology.

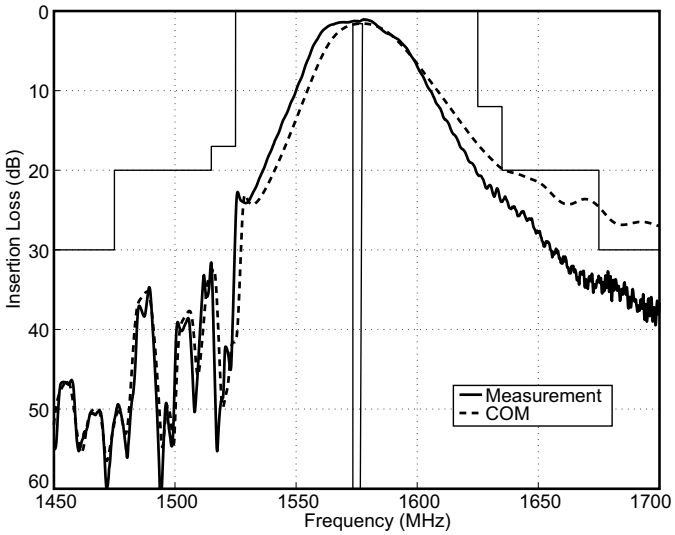

Fig. 12. Measured frequency response (solid curve) and COM simulation (dashed curve) of a 3-IDT balun filter. The minimum insertion loss is 1.07 dB. Specifications shown in the figure are for a low-loss GPS filter.

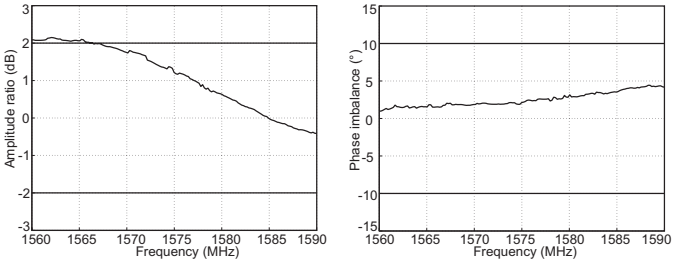

(a) Amplitude imbalance. (b) Phase imbalance.

Fig. 13. Amplitude and phase imbalance of the 3-IDT balun filter in the absolute 3-dB band.

SAW power is effectively transferred from input to output, giving rise to the filter passband. It should be noted that the input power level in Figs. 10(a) and (b) is 20 dBm, whereas in Fig. 10(c) it is 10 dBm. The simulated curves are shifted so that the maximum power coincides with that of the experimental curve.

C. Single-Ended 2-IDT Filter

The experimental frequency response of a 2-IDT filter, along with a COM simulation, is shown in Fig. 11. The curves are shifted 15 MHz down in frequency to allow comparison with the GPS specification. System impedances are 50 Ω with 0.8 pF parallel to both input and output. The experimental curve shows some feedthrough outside the passband, arising from parasitic contact pad capacitances that were not optimized in the design. The main device parameters and experimental results are presented in Table I.

D. Balanced 3-IDT Filter

To obtain balun operation, a 2-track, 3-IDT filter structure was designed. The tracks are similar and connected in parallel with the phases of the outputs inverted with respect to each other. Splitting the structure into two tracks allows for further reduction in resistive losses, as the aperture can be divided between the tracks.

Fig. 12 shows the experimental frequency response of the filter (solid curve). The experimental curve is matched to 60 Ω at the input and 120 Ω at the output, with parallel inductances of 25 nH. A COM simulation is plotted in the same figure, illustrating the excellent agreement between the simulation and experiment. The response is shifted 15 MHz down in frequency to allow comparison with the specification. Figs. 13(a) and 13(b) show the measured amplitude and phase balance characteristics at the output, respectively. The main device parameters and experimental characteristics are summarized in Table I.

If the input of a 3-IDT track is connected to a side IDT and the output to the other side IDT, leaving the center IDT floating, cascaded operation is obtained. Grounding the center IDT makes the operation impossible. A detailed description of such a device is presented in [13].

E. Power Handling of DRF Devices

At the hiccup resonance frequency, a considerable part of acoustic energy is concentrated in the gap area. At high frequencies, the narrow finger structure in the gap area may limit the power handling capability of the device.

As a preliminary test of the power handling of the devices, a 2-IDT filter was driven with 20 dBm nominal input power for 115 hours. The filter was matched such that S_{11} at the resonance frequency was -13 dB. No degradation of electrical performance was observed after this period. In future, more thorough power handling tests should be conducted to establish the power handling capability of the structure.

IV. Conclusion

The novel double-resonance structure presented in this paper enables narrow-band (1%…2%), low-loss filters on leaky-wave substrates. Since the operation of the device is based on the strong resonance arising in the gap region, we conclude that the unsatisfactory performance reported previously in [5] was due to the attenuation in the gap. In the devices studied in this paper, the loss mechanisms in the gap are considerably reduced with the use of distributed gaps, resulting in excellent filter characteristics with minimum insertion loss of 1.07 dB.

Self-matching of the hiccup resonance is important in order to achieve low loss. Obtaining self-matching requires a special condition to be satisfied between the basic COM parameters of the grating. The relation can only be realized on rather strong piezoelectric substrates and for structures having relatively strong reflectivity.

A 2-IDT filter was driven with 20 dBm input power in order to test the power handling of DRF devices. After 115 hours, no degradation in the electrical response of the device was observed. The test indicates that the DRF structure is not extremely sensitive to high power, but it is difficult to make definite conclusions based on these results. Although the power handling capability of a DRF should be comparable to that of a CRF, it may be somewhat limited by the concentration of acoustic energy in the gap area at hiccup resonance. More consistent studies are necessary to establish the maximum and long-time power handling capability of the structure.

Further improvements in the device performance are possible by using double metallization for contact pads, thus reducing the resistive losses and parasitic shunt capacitances, and by introducing modifications in the layout to reduce electrical parasitics.

Acknowledgment

J. Meltaus and K. Kokkonen thank the Finnish Cultural Foundation for postgraduate scholarships. O. Holmgren thanks the Alfred Kordelin Foundation for scholarships.

References

[1] T. Morita, Y. Watanabe, M. Tanaka, and Y. Nakazawa, "Wideband low loss double mode SAW filters," in *Proc. 1992 IEEE Ultrasonics Symposium*, 1992, pp. 95–104.

[2] D.-P. Chen, C. S. Hartmann, S. Kondratiev, V. P. Plessky, and M. A. Sharif, "SAW filter with a coupled SAW impedance element," U.S. Patent 5 610 566, Mar. 11, 1997.

[3] J. Meltaus, V. P. Plessky, S. Härmä, and M. M. Salomaa, "SAW filter based on parallel-connected CRFs with offset frequencies," to be published.

[4] J. Meltaus, V. P. Plessky, S. Härmä, and M. M. Salomaa, "Low-loss, multi-mode 5-IDT SAW filter," *IEEE Trans. Ultrason., Ferroelect., Freq. Contr.*, vol. 52, no. 6, pp. 1013–1019, June 2005.

[5] V. P. Plessky, T. Thorvaldsson, and S. N. Kondratiev, "Degenerated coupled resonator filters," in *Proc. 1996 IEEE Ultrasonics Symposium*, 1996, pp. 25–28.

[6] S. S. Hong, Unpublished, 2004.

[7] W. Wang, X. Zhang, Y. Shui, H. Wu, D. Zhang, and V. P. Plessky, "Minimizing the bulk scattering loss in CRF(DMS) devices," in *Proc. 2004 IEEE Ultrasonics Symposium*, 2004, pp. 1363–1366.

[8] J. Meltaus, V. P. Plessky, and S. S. Hong, "Non-synchronous resonators on leaky substrates," in *Proc. 2005 IEEE Ultrasonics Symposium*, 2005, pp. 2153–2156.

[9] O. Kawachi, S. Mineyoshi, G. Endoh, M. Ueda, O. Ikata, K. Hashimoto, and M. Yamaguchi, "Optimal cut for leaky SAW on $LiTaO_3$ for high performance resonators and filters," *IEEE Trans. Ultrason., Ferroelect., Freq. Contr.*, vol. 48, no. 5, pp. 1442–1448, Sept. 2001.

[10] P. V. Wright, "Analysis and design of low-loss SAW devices with internal reflections using coupling-of-modes theory," in *Proc. 1989 IEEE Ultrasonics Symposium*, 1989, pp. 141–152.

[11] ——, "A review of SAW resonator filter technology," in *Proc. 1992 IEEE Ultrasonics Symposium*, 1992, pp. 29–38.

[12] J. V. Knuuttila, P. T. Tikka, and M. M. Salomaa, "Scanning Michelson interferometer for imaging surface acoustic wave fields," *Opt. Lett.*, vol. 25, pp. 613–615, May 2000.

[13] J. Meltaus, S. S. Hong, and V. P. Plessky, "High-rejection SAW filter based on double-resonance structure," in *Proc. 2006 IEEE Ultrasonics Symposium*, 2006, to be published.

Johanna Meltaus was born in Espoo, Finland, in 1976. She received her Master of Science (in Technology) degree at Helsinki University of Technology (TKK), Espoo, Finland, in 2000, and her Licentiate of Technology degree at TKK in 2002.

She has worked as a Research Assistant in the Low Temperature Laboratory (TKK) and as a Research Scientist in the Materials Physics Laboratory. She is currently working on her Dr.Tech. thesis in the Optics and Molecular Physics Laboratory (TKK). Her previous research interests have included high-temperature superconducting devices and radio holography. Currently she is involved in designing and modeling coupled surface acoustic wave filters.

Ms. Meltaus received the Master's Thesis award of the Finnish Association of Graduate Engineers in 2001, and was awarded the Student Paper Award in the 2005 IEEE Ultrasonics Symposium.

Seong Su Hong received his B.S. and M.S. degree in Materials Science and Engineering at Hanyang University, Seoul, Republic of Korea, in 1994 and 1996. His research topic was the formation of Cobalt silicide for metallization of semiconductor devices.

He worked as SAW Device Design and Manufacturing Engineer at Daewoo Electronic Components Co., Jungeup, Korea in 1996. Since 1999, he joined the SAW development team at Samsung Electro-Mechanics Co., Suwon, Korea. Currently, his main research interest is developing efficient simulation techniques for SAW devices.

Olli Holmgren was born in Espoo, Finland, in 1977. He received the Master of Science (in Technology) degree at the Helsinki University of Technology (TKK), Espoo, Finland, in 2003.

He has worked as a Research Assistant and Research Scientist in the Materials Physics Laboratory (TKK). Currently he is working on his Dr.Tech. thesis in the Optics and Molecular Materials Laboratory (TKK). His research interests include laser-interferometric imaging of the vibrations in surface and bulk acoustic wave devices and in micro-electro-mechanical systems.

Kimmo Kokkonen was born in Helsinki, Finland, in 1977. He received his Master of Science (in Technology) degree at Helsinki University of Technology (TKK), Espoo, Finland, in 2005.

He has worked as a Research Assistant in the Laboratory of Physics (TKK) and as a Research Scientist in the Materials Physics Laboratory. Currently he is working on his Dr.Tech. thesis in the Optics and Molecular Materials Laboratory (TKK). His previous research interests have included instrumentation for a positron life-time spectrometer. Currently, he works on phase-sensitive laser interferometric imaging of the vibrations in surface and bulk acoustic wave devices and in micro-electro-mechanical systems.

Mr. Kokkonen received the Student Paper Award in the 2003 IEEE Ultrasonics Symposium.

Victor P. Plessky (M'93–SM'01) received his Ph.D. degree in physical and mathematical sciences at the Moscow Physical-Technical Institute, Moscow, Russia, and the Dr.Sc. degree at the Institute of Radio Engineering and Electronics (IRE, Russian Academy of Sciences, Moscow, Russia), in 1978 and 1987, respectively. Beginning in 1978, he worked at IRE, first as a Junior Researcher and, from 1987, as Laboratory Director. In 1991, he also worked as a part-time professor at the Patris Lumumba University, Moscow.

He received the full professor title in 1995 from the Russian Government. In 1992, he joined ASCOM Microsystems SA in Bevaix, Switzerland, where he worked as a Special SAW Projects Manager. Since 1997, he has lectured several courses on various SAW topics at Helsinki University of Technology (TKK), Espoo, Finland, as a Visiting Professor. Currently, he holds a docentship at TKK. Since 1998 he has been working at the Neuchatel office (Switzerland) of Thomson Microsonics (later Thales Microsonics, presently Temex Microsonics), from 2002 as a consultant. He has been engaged in research on semiconductor physics, SAW physics (new types of waves, scattering and reflection on surface irregularities, laser generation of SAW), SAW device development (filters, delay lines, reflective array converters), and magnetostatic wave studies.

Dr. Plessky's current interests focus on SAW physics and low-loss SAW filter development. Dr. Plessky is an IEEE Senior Member. He was awarded the USSR National Award for Young Scientists in 1984.